Letters in High Energy Physics Volume 2024
ISSN: 2632-2714

Shape-Selective Self-Assembly and Confinement Dynamics of Colloidal Particles: Exploring Depletion Interactions in Confined Geometries

Sri Charan Yarlagadda,
PhD, Chemical & Biomolecular Engineering,
Georgia Institute of Technology,
St Louis, Missouri,
ysricharanacads@gmail.com

Abstract

This manuscript examines the interactions among colloidal particles, specifically emphasizing depletion and hydrodynamic interactions in confined geometries. The initial section delves into particle-particle and particle-surface depletion interactions, utilizing a combination of numerical modeling and experimental techniques. Current applications of depletion interactions predominantly involve colloidal destabilization for processes like aggregation and filtration. This work, however, models and experimentally demonstrates shape-selective depletion-induced self-assembly, with the goal of fabricating two-dimensional and three-dimensional structures at the nano- and microscale. Through numerical modeling, we calculated the interaction strengths for basic geometries, which informed our experimental strategies to enhance selectivity. These investigations pinpointed crucial parameters and design principles that optimize shape-selective interactions within complex architectures.

The subsequent section presents experimental findings on the confinement dynamics of hard colloids. While the behavior of hard sphere suspensions has been widely researched, understanding their dynamics under confinement is essential. Employing an experimental setup that utilized monodisperse silica spacers to form uniform confinement cells, we measured the hindered diffusivities of hard spheres. Our results indicate that these hard colloids demonstrate consistent behavior across varying levels of confinement. The dynamics of these particles, primarily governed by their rigid structures, highlight important characteristics related to confinement effects, contributing valuable insights into the hydrodynamic interactions of hard spheres.

1. Introduction

1.1 Colloids

A colloidal system forms when one of the basic states of matter—solid, liquid, or gas—is finely dispersed within another. These systems are common in day-to-day life; they are found in blood, paint, smoke, ink, cosmetics, lubricants, pharmaceuticals, and foods such as ketchup, milk, and mayonnaise. Colloids have particle sizes that range from 1 nm to 10 μm and can take various shapes such as spheres, ellipsoids, and rods. Understanding colloidal behavior is essential for improving these products because it allows us to focus on stability; interactions among the particles; flow properties; and transitions between different phases.

Colloidal particles exhibit Brownian motion due to thermal collisions with solvent molecules, leading to random diffusion. Their relatively large size allows observation through techniques like light microscopy, making colloidal suspensions useful for studying complex atomic processes, including nucleation and crystal growth [1][2][3].

This study employs fluorescent spherical colloids (about one micrometer in diameter) to observe colloidal dynamics. It emphasizes the behavior of colloids near surfaces, a focus of interfacial science, where interactions lead to phenomena like templated self-assembly [4] and shear-induced resuspension [5].

Research continues into the interactions between colloidal particles and their environment, which can result in complex microstructures such as self-assembled monolayers and micelles. Key forces influencing these interactions include excluded

volume, electrostatic, and van der Waals forces. This work specifically examines 'non-bulk' colloid-surface interactions, focusing on two main mechanisms: (1) depletion-induced interactions from non-adsorbing polymers and (2) wall hydrodynamic interactions between colloidal particles.

1.2 Forces in colloidal systems

Interactions between surfaces and colloidal particles are crucial for determining the stability and behavior of colloidal systems. Key forces that influence these interactions include van der Waals forces, electrostatic double-layer forces, entropic depletion forces, solvation, and steric forces. The net force on a colloidal particle result from the sum of all forces in a system, often with opposing forces at play. For example, van der Waals forces promote aggregation [1] and can cause emulsions or foams to coalesce [2], while electrostatic double layer forces stabilize emulsions and foams. The interplay between these stabilizing and destabilizing forces is described by the Derjaguin Landau Verwey Overbeek (DLVO) theory [4, 5].

1.2.1 Van der Waals forces

Van der Waals forces are caused due to temporary attractions between molecules and atoms at the atomic or molecular level. They play a significant role in phenomena such as material adsorption (e.g., surfactants), aggregation, and surface tension. These forces are always attractive between identical materials but can be either attractive or repulsive between different materials, depending on the intervening medium.

Van der Waals interactions comprise three components: (i) London dispersion forces, (ii) Keesom orientation forces and (iii) Debye induction forces. The interaction energy of these components decreases with the inverse sixth power of distance. London dispersion forces are typically the most significant due to their presence among all atoms, even in non-polar molecules, acting over distances up to approximately 10 nanometers. For a detailed discussion, readers can refer to Israelachvili [6].

1.2.2 Electrostatic forces

Colloidal particles are often electrically charged, a property that contributes to their stability and resistance to aggregation. The electrostatic double layer around these particles produces a repulsive force that keeps them from coming into close contact and aggregating. The key electrokinetic phenomena of electrophoresis, electroosmosis, and streaming potential in colloidal systems are all driven by the electrostatic double layer. The zeta potential (ζ) is a measure of the level of surface charge on a particle and thus an indicator of colloidal stability.

Surface charges can arise from mechanisms like the ionization of surface groups [7] or adsorption of charged species such as polyelectrolytes or ionic surfactants [8]. The surface charge alters the surrounding ion distribution, attracting counterions and forming an electrical double layer, which balances the Coulombic attraction and osmotic repulsion. Although the system remains electrically neutral overall, the electrostatic double layer has two distinct regions: the Stern layer (composed of tightly packed ions) and the Gouy-Chapman layer (which contains more loosely associated ions).

The thickness of the diffuse Gouy Chapman layer is represented by the Debye screening length (κ^{-1}), which decreases as the concentration of electrolytes increases. Although we do not delve into the mathematical details here, charged surfaces are usually described in terms of surface charge density (σ) and surface potential (ψ_0). If one wishes to examine either the potential variation from the surface or the ion distribution in the solution, one must solve the Poisson Boltzmann equation. This equation—a non linear, second order partial differential equation—predicts that under conditions of low and constant surface potential, potential will decay exponentially with distance (x) from the surface.

$$\psi \approx \psi_0 e^{-\kappa x} \tag{1.1}$$

The below equation can be used to calculate Debye length:

$$1/\kappa = \left[\frac{N_A e^2}{\varepsilon\varepsilon_0 k_B T}\sum_i z_i^2\, c_i^{\infty}\right]^{-1/2} \qquad (1.2)$$

where c_i^{∞} represents the concentration of ions of type iii, while N_A is Avogadro's number, e denotes the electronic charge, and z_i is the valency of the ion. The dielectric constant for a medium is given by $\boldsymbol{\varepsilon}$, and ε_0 stands for free space permittivity. The term $k_B T$ is the product of the Boltzmann constant k_B and the temperature T. All ion species present in the solution are included in the summation.

The Debye screening length relates inversely to both the concentration and valency of the electrolyte. Thus, it becomes longer (meaning that the potential decays more slowly) as either parameter decreases. When the potential is large, Equation 1.1 becomes invalid. For those situations, solving the Poisson Boltzmann equation gives a better picture of how the potential changes with distance from a surface.

In this work, Stern theory was used for numerical formulations instead of Gouy Chapman theory, as it offers a more refined approach and by distinguishing between the total double-layer potential (ψ_0) and the potential at the diffuse layer (ψ_d). Employing Stern theory, along with the linear superposition approximation [9] and the Derjaguin approximation, the repulsive interaction energy between two spheres (Ω^{ss}) of radius R can be expressed as follows:

$$\Omega^{ss} = 64\pi R\, k_B T n^{\infty} \kappa^{-2} tanh^2\left(\frac{ze\psi_0}{4k_B T}\right)\exp(\quad) \qquad (1.3$$

x denotes the separation distance between the two spheres. To properly model the overall colloidal interaction between two particles, it is necessary to understand their electrostatic interaction energy. In the next section, we will show how to combine the interaction potentials of colloidal systems to explain qualitatively their behavior as a function of separation distance.

1.2.3 Forces in colloid-polymer mixture

In the case of a binary colloid-polymer mixture, various forces may arise depending on the interaction between colloidal particles and polymer molecules. When polymers are introduced into a colloidal suspension, two primary scenarios can occur: (a) polymer molecules adsorb onto the colloid surface, where they can either induce attractive bridging forces or steric repulsive forces, the latter resulting from the unfavorable entropic penalty associated with the compression or overlap of polymer chains, or (b) the polymer molecules remain non-adsorbing. In the latter case, the polymers, often modeled as random coils with a radius of gyration R_g, behave like smaller colloidal particles, giving rise to depletion interactions, which are entropic in nature, between the larger colloidal particles.

When the distance between two large colloidal particles becomes smaller than the hydrodynamic diameter of the polymer, the exclusion of polymers from the region between the colloids leads to an anisotropic distribution of osmotic pressure, creating an attractive depletion force between the colloids. Much of our research has focused on depletion interactions in colloid-polymer mixtures [10, 11]. Section 2 introduces a versatile new method for calculating the depletion potential between hard spheres and various simple and complex geometries, where the depletion interactions are discussed in greater detail. Section 3 presents experimental studies investigating these depletion interactions.

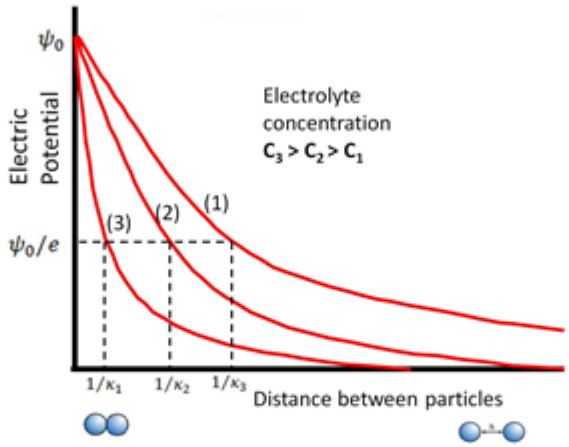

Figure 1.1 Potential as a function of distance between the particles. Debye length $(1/\kappa)$ is the distance at which the potential, ψ_0 has dropped to (1/e) of its value at the surface ψ_0.

1.2.4 Miscellaneous forces

Additional forces of significance in colloidal systems include solvation forces (such as hydrogen bonding) and hydrophilic/hydrophobic interactions. At extremely short distances (a few nanometers), solvation forces come into play when a liquid becomes confined in a narrow gap between two surfaces. These forces can exceed the strength of DLVO forces and therefore cannot be overlooked. Solvation forces are mainly the result of solvent molecules forming semi-ordered layers between surfaces, leading to repulsion when hydrated groups on the surfaces come close to each other. Such stabilizing short-range forces have been observed between solid surfaces like silica and mica in water [12, 13] and have been shown to stabilize soap films in saline environments [14] and affect biomembrane interactions [13]. These short-range repulsive forces have been implicated in preventing coagulation at very small separations.

Hydrophilic/hydrophobic forces also play a critical role in colloidal behavior. These forces originate from the strong electrostatic cohesion of water molecules, which form hydrogen bonds with each other while excluding non-polar molecules incapable of hydrogen bonding, such as alkanes, hydrocarbons, and fluorocarbons. Consequently, substances like hydrocarbons and halocarbons are poorly soluble in water and separate into distinct phases due to the "hydrophobic effect."

1.3 Effective interaction potential in colloid-polymer mixtures

In addition to DLVO interaction potentials, colloidal particles experience entropy-driven depletion forces, which can be attractive or, in some cases, repulsive when non-adsorbing polymers are present. Thus, the overall effective potential in these systems should be viewed as the sum of the van der Waals attraction potential, the electrostatic repulsion potential (assuming the presence of charged particles and surfaces), and the depletion potential (refer to Figure 1.2). Throughout the subsequent sections, we will explore methods to manipulate the effective potential to align with our research objectives. It is crucial to comprehend the characteristics of the effective interaction potential within binary colloid-polymer mixtures.

Let's consider the effective interaction potential between two colloidal particles or between a colloidal particle and a surface. At large separations, the individual potentials diminish to zero due to negligible interactions, resulting in an insignificant effective potential. However, as the distance between the particles decreases, a pronounced minimum in the combined effective potential energy emerges, primarily due to the strong van der Waals attraction between the surfaces. Just beyond this region lies an electrostatic repulsive barrier, where the electrostatic repulsion potential predominates over the van der Waals attraction. It is important to

note that this repulsion arises not directly from the surface charge on the particles but rather from the interactions between the two double layers. Our goal is to ensure that the electrostatic barrier is sufficiently strong to prevent permanent aggregation of particles within the van der Waals minimum.

The secondary minimum depicted in the figure arises from the influence of depletion potentials, which become significant at this separation distance. If a secondary depletion minimum is established, the effective particle interaction potential can be tailored to achieve various types of particle-particle or particle-surface interactions, as discussed in the further sections.

1.4 Hydrodynamics of hard colloids

Section 1.2 addressed different static forces in colloidal suspensions. In contrast, hydrodynamic forces are dependent on the movement of colloidal particles in relation to their surroundings. These forces originate from the interactions among incompressible fluid molecules, influenced by the Brownian motion of other colloids or solid surfaces, demonstrating the reciprocal relationship between particles and fluid flow.

Unlike van der Waals and electrostatic forces, which primarily impact colloidal scales, hydrodynamic forces also play a significant role at larger scales, where momentum transfer and boundary conditions come into play. For instance, a swimmer creates flow in still water but experiences increased drag in a confined pool due to reflected disturbances. Likewise, hydrodynamic forces are crucial for determining particle mobility and fluid behavior at the colloidal scale. In dense suspensions, the effective viscosity and mobility of hard particles are shaped by hydrodynamic interactions and particle-to-particle interactions [15]. The interactions among colloidal particles, as well as with nearby walls, directly influence local fluid flow.

Under low Reynolds number conditions, the Stokes-Einstein relation describes the behavior of unbounded hard spherical particles in a dilute state based on their hydrodynamic radius:

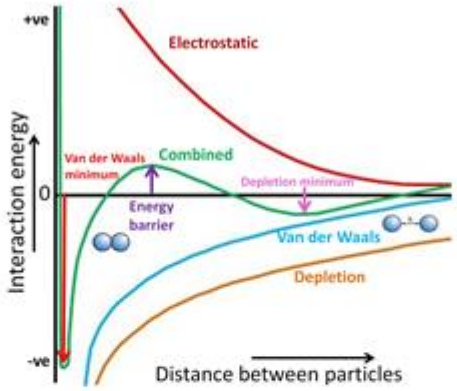

$$D = \frac{k_B T}{6\pi\eta R_H} \quad (1.4)$$

Figure 1.2 The schematic illustrates the interparticle potentials for colloidal pa van der Waals (blue), electrostatic (red), and depletion (brown) interactions, a interparticle potential (green). The figure highlights both the depletion and van

where η represents the medium viscosity, D is the free diffusivity of the particle, T is the temperature, and k_B represents Boltzmann constant. By assessing the hydrodynamic drag on particles freely diffusing in an open system, valuable physical insights can be gathered about the particles and the local fluid they explore. Detailed discussions

regarding these measurement techniques will be provided in the next section.

Although the Stokes-Einstein relation is widely accepted for hard spheres, the concept of true hard spheres is debated. Some researchers have highlighted the intrinsic softness in systems resembling hard spheres [16, 17], leading to inquiries about what constitutes "hardness" in colloidal particles. When particles approach each other or a solid interface, the thinning lubrication film requires the fluid to escape, prompting the question: "What defines softness?" This notion can be examined from multiple perspectives, such as particle elasticity, porosity, types of soft interactions, and volume fraction. In this context, softness refers to attributes that allow lubrication fluid to exit from gaps.

Understanding the hydrodynamic interactions of hard particles is essential for numerous applications, such as emulsion stability [3], particle filtration [21], migration through porous media [22], and flow within microfluidic channels [23].

This work emphasizes particle-wall hydrodynamics, focusing on how these interactions affect the movement of hard particles in both free and confined environments. While the Brownian motion of free particles is well characterized, the presence of solid walls complicates the dynamics due to restricted flow fields, which impact particle mobility. Consequently, Brownian diffusion is significantly hindered in proximity to walls. Pioneering work by Brenner [19] and Goldman et al. [24] established hindrance coefficients for hard spheres near walls using lubrication theory. One experimental approach involves measuring the diffusion hindrance caused by walls across different confinement levels, enabling the determination of hindrance coefficients as a function of confinement. In our studies, we employ polystyrene microspheres as our primary hard colloids.

1.5 Particle tracking video microscopy

In the past decade, microrheology has emerged as a vital technique for studying complex fluids at smaller length scales, using various experimental methods to determine their rheological properties [25, 26]. Unlike traditional macrorheology, which operates at millimeter scales, microrheology allows for the analysis of smaller sample volumes, making it especially useful for expensive or biologically sensitive fluids. However, differences can occur between properties measured with microrheology and those from macrorheology, highlighting the unique approaches used in each.

Particle tracking video microscopy (PTVM) is a microrheological method that utilizes the motion of colloidal probe particles to investigate their behavior and the rheological characteristics of their environment. PTVM experiments fall into two categories: active microrheology, which manipulates particles with external forces, and passive microrheology, relying on the Brownian motion of particles due to thermal fluctuations. While passive microrheology focuses on linear properties, active microrheology examines nonlinear viscoelastic properties by applying forces that disrupt equilibrium. In both cases, PTVM tracks particle trajectories to calculate mean-squared displacements, which provide insights into diffusivities, viscosity, frequency-dependent shear modulus [27], solvent temperature [28], hydrodynamic radius, and microstructural morphology [26].

PTVM has applications across various fields, including biophysics, living cells, microfluidics, colloidal physics, rheology, and polymer science. It provides both ensemble-averaged and locally resolved data from individual colloidal probes. This work primarily emphasizes passive PTVM, which involves four steps: recording videos of diffusing colloidal particles, identifying particles in each frame using custom algorithms, compiling individual frame data into particle trajectories, and performing statistical analyses to derive physical insights [29].

Various groups have created specialized computational algorithms for particle detection, which can be grouped into four main types: cross-correlation, sum-absolute difference, centroid, and direct Gaussian fit [30]. The centroid and direct Gaussian fit methods determine particle positions from individual frames, while the other techniques involve comparing consecutive frames. The centroid method is noted for its robustness against noise, particularly for micron-sized particles. Our research

utilizes a brightness-weighted centroid algorithm created in Interactive Data Language (IDL).

A typical PTVM experiment begins with observing probe particles' Brownian motion using an optical microscope, recording with a CCD camera at 30 frames per second and 640 × 480 pixel resolution. Each video consists of about 1,500 images, amounting to approximately 440 MB. Given the small displacements from Brownian motion and high sensitivity to noise, experiments are performed on a vibration-isolated optical table. Analyzing the recorded videos with IDL software involves four steps: image restoration, locating potential particle centers, refining positions, and linking them to form trajectories [29].

The recorded images often suffer from noise, which can be reduced using algorithms [31]. The first step addresses spatial frequency noise and large background noise to enhance contrast. The second step identifies potential particle centers using multiple brightness-weighted centroids. The third step refines these positions using criteria like eccentricity and brightness thresholds to eliminate out-of-focus or elongated particles. The fourth step links particle positions to create trajectories, which are then statistically analyzed to reveal the mechanical and physical properties of the colloidal suspensions. The mean squared displacement (MSD) is calculated as a function of lag time (τ).

For Newtonian fluids, the Einstein-Stokes relation correlates MSD, mechanical properties, hydrodynamic radius, and temperature. Thus, the MSD of particles is expressed as:

$$MSD = \frac{dk_B T}{3\pi\eta R_H}\tau \qquad (1.5)$$

Here *d* represents the dimensionality. A linear relationship can be proposed using equation (1.3.1) with the slope being:

$$slope = \frac{MSD}{\tau} = \frac{dk_B T}{3\pi\eta R_H} = 2dD \qquad (1.6)$$

With the above equation, the ensemble-averaged diffusivities of colloidal particles can be easily calculated from the slope of the MSD versus lag time plot. From this, the viscosity (*η)* can be determined.

$$\eta = \frac{d \cdot k_B \cdot T}{3 \cdot \pi \cdot R_H \cdot slope} \qquad (1.7)$$

Using PTVM, the viscosity of a Newtonian fluid can be determined if the hydrodynamic radius of the colloidal probe particle is known, as all other variables in equation (1.4.3) can be established or measured. This work will utilize these relationships to estimate both free and hindered diffusivities as well as viscosities of colloidal particles and solutions, through the analysis of the mean squared displacement (MSD) versus lag time plot.

1.6 Motivation and structure of this work

This work investigates 'non-bulk' interactions between colloids and surfaces, emphasizing two primary phenomena: depletion interactions and hydrodynamic forces. By carefully optimizing depletion interactions, colloids can be organized on surface microstructures, promoting directed self-assembly at micro and nanoscale levels. Yodh and collaborators were pioneers in demonstrating how small particles can trap larger colloids at sharp edges on surfaces [32]. Subsequent research utilized depletion forces for depositing particles on patterned templates [33] and anisotropic structures [34], showcasing potential for cost-effective fabrication of self-organizing materials. Additionally, depletion interactions have opened avenues for innovative applications, such as fractionating bidisperse colloidal systems [11] and new particle separation methods [35]. The emergence of organized configurations from adding non-adsorbing polymers to colloidal suspensions is particularly noteworthy.

2. Modeling of depletion attractions in confined surfaces

Self-assembly is the natural process where building blocks spontaneously organize, enhancing system

internal structure. This phenomenon, observed in biological systems like lipid bilayers [42] and DNA folding [43], can be replicated artificially, offering a scalable method for creating complex nanoscale structures, unlike traditional top-down lithography techniques that are costly and slow [44]. In colloidal systems, smaller nanoscale colloids, known as depletion agents, can induce depletion attractions between larger colloids, leading to hierarchical assembly dynamics.

Depletion interactions, driven by entropy, are prevalent in crowded colloidal environments where small species like polymers occupy significant volumes. These forces are critical in natural substances (blood, milk, clay) and various industrial applications, influencing the stabilization and transport of colloidal dispersions [11]. The addition of smaller particles significantly alters the dynamics and properties of colloids by introducing depletion interactions. In this work, the focus is on depletion interactions induced by polymers in colloid-polymer mixtures, using the term "small-spheres" loosely for theoretical modeling.

Depletion forces arise from the excluded volume around larger particles, creating an entropic driving force that minimizes this volume. This overlap encourages larger colloids to come together, increasing the accessible volume for smaller particles and their entropy. Notably, these interactions can generate ordered phases for hard spheres, with the potential to form stable colloidal liquid phases before crystallization occurs, depending on the colloid-polymer size ratio [48].

Since depletion interactions are entropic, they are material-independent and can involve various depleting agents, including polymers and proteins, as long as they do not adsorb onto larger colloids. This work explores the theory and numerical modeling of these interactions in two sections, assessing their feasibility for self-assembly experiments and how numerical findings support experimental results

Adding small spheres or polymers can enhance the order of larger spheres, impacting phase behavior with practical implications across various materials, from frozen desserts to paints [53]. Depletion forces play a role in applications such as wastewater treatment [54], beverage clarification [55], and protein solution processing [56]. The aim of this study is to investigate the dynamics of colloid-polymer mixtures on structured surfaces for depletion-induced self-assembly, potentially leading to scalable manufacturing methods. Notably, Yodh and coworkers demonstrated the use of small spheres to manipulate larger colloids, facilitating their confinement to two-dimensional spaces adjacent to walls [53]. This approach combines entropic forces with patterned templates to create two- and three-dimensional structures, paving the way for novel nanoscale architectures in fields like photovoltaics and optoelectronics [58].

Asakura and Oosawa (1958) were the first to identify the depletion effect occurring between two bodies submerged in a solution of rigid spherical macromolecules [10]. They modeled the rigid small spheres as an ideal gas at low concentrations and developed a straightforward analytical model to describe the interaction potential in basic sphere-sphere geometry, expressed as follows:

$$U(r) = \frac{4\pi}{3}(R_L + R_S)^3 \left(1 - \frac{3r}{4(R_L + R_S)} + \frac{r^3}{16(R_L + R_S)^3}\right) \Pi \quad (2.1)$$

Here R_L, R_S and r denote the larger sphere radius, smaller sphere radius and the center-to-center separation. The Osmotic pressure (Π) of the small-spheres in suspension is described by the dilute gas law, $3\Phi T/4\pi {R_s}^3$ where Φ is the volume fraction of the small-spheres. According to the Asakura and Oosawa (AO) model, the attractive energy between two bodies is proportional to both the volume fraction of the smaller spheres and the ratio of the diameters of the larger and smaller spheres. In this model, rigid small spheres can also represent non-adsorbing (ideal) polymer molecules [11]. To account for variations in overlap volume, geometric correction factors are introduced to improve the equation. Since the small rigid spheres are thermodynamically ideal, the osmotic pressure is given by Van 't Hoff's law:

$$\frac{\Pi}{c} = \frac{RT}{M} \quad (2.2)$$

where $\boldsymbol{c}$ represents the concentration (grams of solute per liter), M represents the molecular weight of the solute, R represents the gas constant and T is the temperature of the system. The term "thermodynamically ideal" refers to a theoretical solution where solvent-solvent, solute-solvent, and solute-solute interactions are uniform. For dilute and semi-dilute polymer solutions, these "ideal-gas-type" models can serve as reasonable approximations of the physical system. However, for non-ideal conditions, this relationship can be expressed as a general power series expansion in c given by:

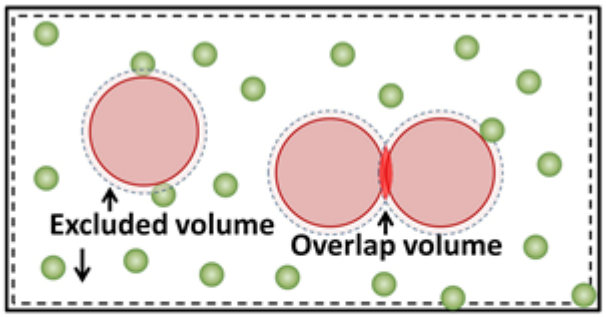

$$\frac{\Pi}{c} = RT\left[\frac{1}{M} + A_2 c + A_3 c^2 + \cdots\right] \quad (2.3)$$

Figure 2.1 Depletion attractions between large-spheres in a suspension of small-spl

A2 and A3A_3A3 are the second and third virial coefficients, which can be empirically determined for a specific solute-solvent system. Numerous researchers have built upon these models to address their specific issues of interest [50, 59]. At low concentrations of small spheres, various simple depletion models (Asakura & Oosawa 1958; Vrij 1976; Gast et al. 1983) [50, 59] are based on the idea that the attraction potential is directly proportional to both the volume fraction of the small spheres and the ratio of large to small sphere diameters.

An alternative approach to derive the interaction potential is by utilizing the extended Gibbs adsorption equation, which indicates that the Helmholtz free energy of a colloid-polymer mixture decreases by $\Pi \times \Delta V$ (ΔV being the overlap volume) as the particles move closer together [11]. This method offers the benefit of directly correlating particle depletion with the depletion interaction potential, and it provides approximate formulas for the interaction potential when precise calculations are not feasible.

Numerous studies have validated the Asakura-Oosawa (AO) theory experimentally. Yodh et al. found that their data fit well with the AO theory at low small-sphere volume fractions (Φ = 0.04-0.07). However, at higher concentrations, the liquid structure of small spheres becomes significant, leading to effects like substantial depletion repulsion (Φ > 0.1) or even oscillatory interactions ($\Phi \geq 0.25$) at separations near one small-sphere diameter. Evidence for these repulsive interactions has been demonstrated through both experimental and numerical research [45, 64, 65].

The AO theory, based on entropic arguments, does not predict these repulsive interactions, while an alternative osmotic pressure interpretation suggests that high small-sphere concentrations cause repulsion at these separations. Long-range oscillating depletion forces have been observed in charged macromolecule systems, possibly due to pair-potential correlations among the macromolecules [66, 67]. Bechinger et al. identified repulsive depletion forces in binary hard-sphere

mixtures with high size ratios, even at low polymer concentrations, attributing these effects to van der Waals forces that elevate polymer concentrations near large-sphere surfaces. Consequently, the AO theory is less applicable in these scenarios and is best suited for cases where smaller species are inert.

In our research, we will employ the AO model for interactions where the polymer concentration is significantly below the overlap concentration and van der Waals forces are negligible. The AO model is based on several assumptions: large colloids are treated as hard spheres, and non-adsorbing polymers are considered small spheres that are interpenetrable but cannot penetrate large spheres. This model accurately represents colloid-colloid interactions for both sterically stabilized and charged colloids in high ionic strength solvents.

The interpenetrability assumption holds for polymers in theta-solvents and good solvents, described by the ideal chain model, which allows monomers to occupy the same space without excluded volume effects. Meijer and Frenkel demonstrated that the AO model is effective if the radius of gyration of polymers is less than 70% of the large colloids' radius, particularly in dilute solutions. In these systems, the depletion overlap thickness on large spheres and walls correlates with the polymers' radius of gyration.

A critical factor is the overlap concentration, above which polymer entanglement effects occur, invalidating the AO model. Joanny et al. (1979) highlighted that the correlation length, which is the average distance between neighboring entanglement points, becomes relevant in this regime. For non-adsorbing polymers in the overlap region, depletion attractions persist, but the overlap thickness now relates to the correlation length rather than the radius of gyration.

In conclusion, the AO model treats ideal polymer chains as penetrable hard spheres with a diameter of $2R_g$. It accurately predicts depletion effects in dilute polymer solutions with low concentrations of small spheres, though repulsive forces may emerge at higher concentrations. For non-adsorbing polymers with excluded volume effects, the overlap thickness depends on the size ratio R_L/R_g and the polymer concentration.

2.1 Other important Interactions

In addition to depletion interactions, two other forces influencing colloidal interactions are Van der Waals forces and electrostatic forces. Van der Waals forces become particularly strong at short distances between particles, allowing charged colloidal particles to overcome electrostatic repulsion and form aggregates. However, this work focuses on other aspects, so Van der Waals forces will not be modeled. Section 1 discusses electrostatic interactions between particles, but the interactions between particles and wall surfaces are not covered in this work. The repulsive electrostatic interaction energy between charged spheres (Ω^{ss}) is given by:

$$\Omega^{ss} = 64\pi R_L\, k_B T n^{\infty} \kappa^{-2} tanh^2\left(\frac{ze\psi_0}{4k_B T}\right) \exp(-\kappa x)$$

where n^{∞} represents the concentration of the electrolyte in the bulk solution, κ^{-1} denotes the Debye screening length, z is the electrolyte's valency, ψ_0 indicates the surface potential, x denotes the distance between the two surfaces, k_B denotes the Boltzmann constant and T refers to the temperature. This equation illustrates how the repulsive interaction energy is affected by the electrolyte concentration, as the binding of counterions to the charged sphere surfaces reduces the surface potential ψ_0. Consequently, lower surface potentials result in weaker repulsive energies. The intensity of electrostatic repulsion influences both the depth and position of the attractive depletion potential well, which ultimately affects the separation between colloids and surfaces and impacts the associated excluded overlap volume.

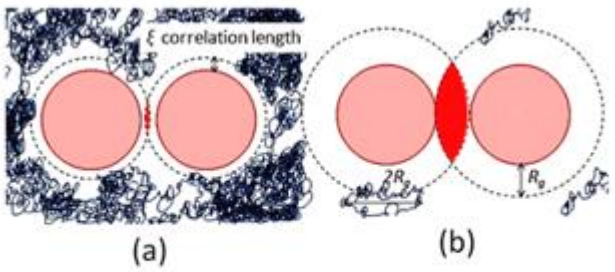

Figure 2.2 Overlap thicknesses characterized by: a) the correlation length in the overlap concentration regime, and b) the radius of gyration in the dilute regime.

2.2 Selectivity of depletion attractions

The primary goal of this work is to achieve high selectivity in depletion attractions to facilitate the preferential deposition of large spheres on specific geometries, while avoiding unwanted interactions or aggregation in the bulk. We aim to determine if the interaction parameters can be finely tuned to enable colloidal particles to interact beneficially with designated features on 2D/3D substrates, without causing bulk aggregation or unwanted adhesion to flat surfaces. Previous research by Yodh and Dinsmore demonstrated that by adjusting the concentrations of spheres and non-adsorbing polymers, they could prevent bulk crystallization while promoting surface crystallization [50]. Sacanna, Pine, and colleagues achieved high selectivity by carefully tuning interactions between specially designed dimpled (lock) particles and smaller (key) spheres, ensuring that key particles only bound to the concave cavities of lock particles, as illustrated by the greater overlap volume with the concave dimple than with the convex surface [51].

Our focus is on self-assembly processes at a larger scale, where numerous particles interact with substrates featuring specific geometric characteristics to create new colloidal structures. Key questions include whether depletion interactions can be fine-tuned on a larger scale and whether they can underpin controlled nanoscale self-assembly.

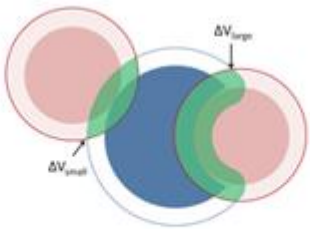

Figure 2.3 A diagram showing the lock-key colloid interactions. Small-sphere interactions are more likely to happen in the cavities due to higher volume overlap.

Research has demonstrated the feasibility of forming well-ordered structures through depletion interactions. For instance, Dinsmore et al. self-assembled colloidal particles on the step edges of a silicon wafer, directing particles to form ordered structures at corners before filling flat walls or bulk areas [50]. While literature supports the possibility of selective depletion attractions, comprehensive analyses of geometric structures needed for maximizing desirable interactions are limited. Lin et al. illustrated the potential to create arrays for self-assembly in the grooves of grating templates [38].

To gain a quantitative understanding of selective deposition, we will perform modeling studies focused on self-assembly of colloids induced by controlled depletion on structured surfaces. Different surface geometries can attract colloidal particles, and the strength of the interactions—whether between particles or between particles and surfaces—depends on the overlap volume, which is affected by the contact geometry. As illustrated in a

diagram, the attraction strength increases from case A to case E due to progressively larger excluded volume overlaps. For instance, a particle with an edge exhibits a significantly greater overlap volume than a flat wall, indicating stronger particle-edge attractions. To adjust the interaction strength, we will modify two critical parameters: (1) the size of the small spheres, which determines the depletion zone thickness, and (2) the number density (volume fraction) of these spheres, which influences osmotic pressure. This understanding, combined with electrostatics, will inform our modeling and experimental approaches to investigate shape-selective interactions.

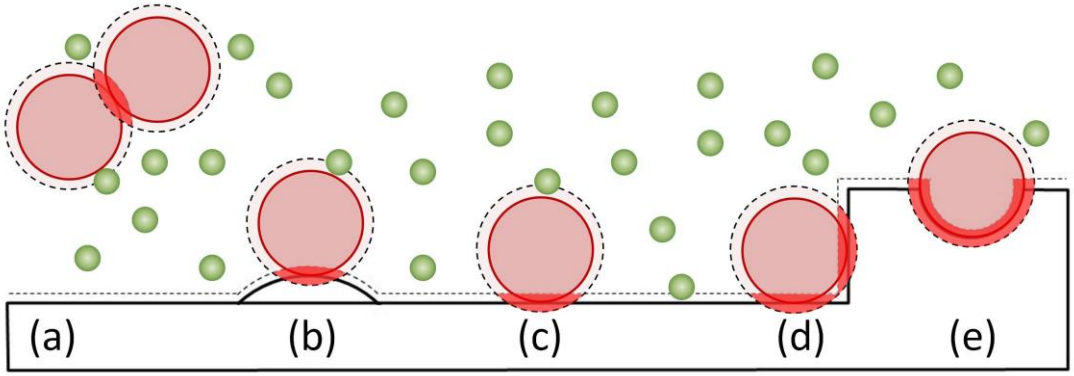

Figure 2.4 Illustration of depletion attraction across different geometries of interest. The dashed lines indicate the excluded volume, with the shaded region representing the overlap, which is directly related to the strength of the interaction. In panel (a), two large colloidal spheres are depicted. To the right, interactions between a sphere and a solid wall are shown for various wall geometries: (b) ridge, (c) flat wall, (d) edge, and (e) cavity.

2.3 Numerical approach

A numerical code was created in MATLAB to compute the shape specific excluded volume overlap. From this, we derived the depletion interaction potential for the Asakura & Oosawa (AO) model parameters. Our model colloidal particles interact with axially symmetric surfaces of arbitrary geometry. This includes objects with simple shapes, like cylinders, and those of greater complexity. Both kinds of surfaces give us insight into how feasible it is to conduct the needed experimental work. The surfaces along which the model colloidal particles and the axially symmetric shapes make contact are the boundaries that the numerical code follows.

We use a versatile numerical method to calculate depletion interactions between two axially symmetric non spherical colloids, which is described in subsequent sections. This method integrates with the AO model, allowing us to estimate the depletant induced interaction potentials between various geometric shapes in different dimensions. A primary advantage of the approach is it helps pinpoint design criteria for exploiting shape selective interactions between relevant geometries.

For geometric shapes that are symmetric about an axis (that is, geometries with axial symmetry) or that are symmetric about a point (that is, spherical geometries), the overlap area can be represented in a completely different way. We can consider the area of overlap to be the area formed by two intersecting circles—one circle representing the volume of a single particle and the other circle representing the volume of the second particle. This way of deducing volume exclusion is easier, and I would argue it is more intuitive. It is much easier to think in terms of cross sections along the axis of symmetry and in terms of the shapes of 2D figures formed by intersecting "circular" particles.

We derived a general numerical solution to find the intersection area of two circles with different radii. This was done by taking into account the distance between their centers and their radii. The overlap area formula was developed and validated, and it is also available in the "Circle Circle Intersection" section on the Wolfram MathWorld web resource [80]. We implemented a MATLAB code to execute these algorithms and help us study the intersection areas of circles.

We used a similar approach to compute interaction potentials for both simple and complex contact

geometries. We started with straightforward cases, such as sphere sphere, sphere wall, and sphere edge interactions, which are shown in Figure 2.4. For these cases, we computed the overlap volumes and used them in our potential energy calculations.We started with simple shapes and then looked at more complex three dimensional forms, like uniform cylindrical surfaces, which are good stand ins for basic nanowires. We even examined how different shapes of nanowires—like ones with varying diameters—interact with spherical particles. The potentials we calculated for these interactions show a clear trend: the strength of the attractive forces between the colloidal particles increases in a straightforward way from the basic sphere sphere interaction up to the more complex edge interactions of the two particles. To give you a specific idea of just how much stronger one interaction is compared to another: For certain sizes of our colloidal particles and polymers, at a set concentration of those polymers, we found that the attractive potential between a particle and an edge of its partner is exactly twice that for a particle wall interaction and about four times that for just two spheres interacting.

Similar numerical estimates were reported by Yodh et al. in their studies on the selective deposition of particles on flat wall and edge surfaces [58]. In Section 3, we will show that this ranking order aligns with experimental results, although it is important to note that we did not conduct direct measurements of the entropic potentials of mean force.

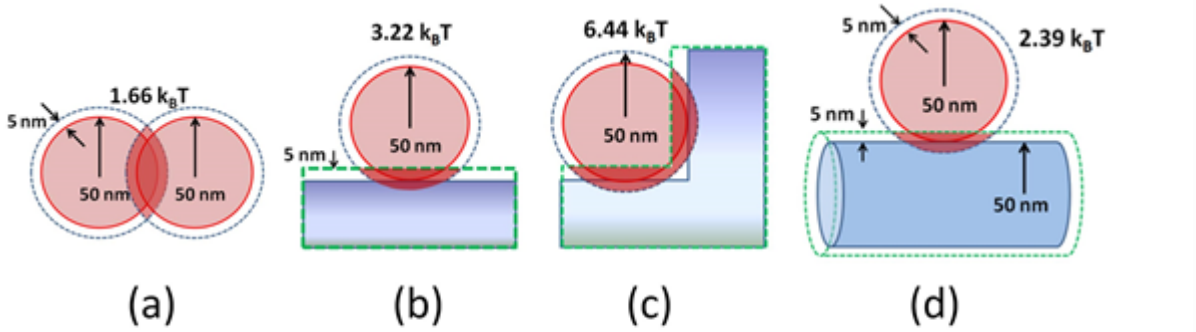

Figure 2.6 The schematic depicts the depletion interaction (R_s = 5 nm, R_L = 50 nm at a small-sphere concentration of 0.38 wt %) occurring between (a) two large colloidal spheres and between a sphere and a solid wall across various geometries: (b) flat wall, (c) edge, and (d) cylinder. The interaction strengths, moving from left to right, are are 1.66 k_BT, 3.22 k_BT, 6.44 k_BT and 2.39 k_BT.

When investigating the self-assembly of colloids into intricate 2D and 3D shapes, we aim to use this process to direct particles onto specific sites of those shapes. A major hurdle in doing this with depletion interactions is making those interactions selective. We can partially achieve this by using the shapes themselves as a means to encode selectivity. Perfectly fitting surfaces maximize excluded volume overlap—an essential ingredient for deposition at intended sites. Poorly fitting surfaces reduce it—a condition unfavorable for site directed assembly.

Lin et al. have demonstrated...The potential of using a periodically patterned template to form arrays of structures has been shown to be effective for the self-assembly of colloidal particles at exact positions on the template. Sacanna, Pine, and others have reached an impressive level of selective interactions with specially designed lock particles. They demonstrated that smaller spheres fit perfectly into the cavities of these lock particles, while interactions with the convex exterior were unsuccessful [51].

If we can show that particles can be deposited at specific points on our complex intended geometries, we will be much closer to a new way of thinking about nanoscale three-dimensional architecture. In the next section, we will model interactions between spherical particles and nanowires with modulated diameters. We will conduct our first studies using both step change and sinusoidal diameter modulation before moving on to non-spherical geometries for both interacting "particles."

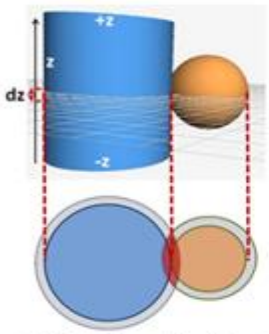

a) *Circle-Circle area of overlap*

$$A_{overlap} = A(R_1, d_1) \cap A(R_2, d_2)$$

b) *Excluded volume overlap*

$$V_{overlap} = \int_{+z}^{-z} A_{overlap} dz$$

Figure 2.5 The figure illustrates the cross-section of the intersection between a cylinder and a sphere, resulting in circular overlaps. On the right, a two-step algorithm is presented for calculating the total excluded volume overlap.

2.3.1 Spherical particles on undulating cylinders

This study focuses on designing interactions in undulating nanowires with sinusoidal diameters to ensure particles deposit in the grooves while preventing unwanted aggregation and adhesion to the ridges. We aim to achieve depletion-induced self-assembly for precise deposition of colloids along the nanowire's sidewalls, targeting shape-selective interactions of 5 k_BT or higher, while keeping undesirable interactions below 2 k_BT.

These interaction thresholds are based on findings that successful depletion interactions for isotropic spheres exceed 5 k_BT, while attractions weaker than 2 k_BT can be disrupted by thermal fluctuations, leading to particle resuspension [81][82]. Calculations for the depletion potential of spherical colloids at specific curvature points on the nanowire were conducted, with details illustrated in Figure 2.7.

Polyethyleneglycol (PEG, MW = 11,500 Da; $R_s = R_g$ = 5 nm) [83] was selected as the non-adsorbing depleting polymer, as it has been effectively used in previous research to generate depletion interactions [70][81]. The spherical colloids, referenced in section 3, were made from polystyrene (PS) but can be fabricated from other materials as long as they do not interact with PEG.

In a theoretical aqueous solution containing both the depleting agent and colloids, particles diffuse toward the nanowire, requiring modeling of shape-selective interactions that allow particles to bind in grooves while failing to adhere to ridges. The model parameters (R_L/R_g, R_g and Φ) were adjusted to achieve a particle-groove interaction strength of 5.0 k_BT, with the particle-ridge interaction at 1.8 k_BT, insufficient for permanent deposition. An intermediate scenario yielded a strength of 2.7 k_BT, suggesting that particles may drift towards the grooves if initial binding is not permanent.

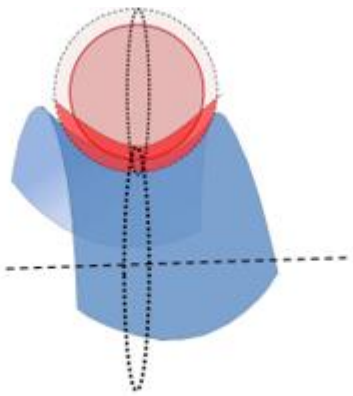

Figure 2.8 A three-dimensional depiction of the sphere-saddle configuration shows the interaction between a sphere and the groove of the undulating nanowire.

These strengths were modeled for a PEG concentration of 0.38 wt%, well below the 5 wt% overlap concentration [84]. The numerical modeling assessed the excluded overlap volume for three contact scenarios by breaking down the geometry of the undulating cylinder and calculating each interaction potential separately. For instance, the overlap volume for the particle-groove was modeled as saddle geometry (refer to Figure 2.8).

Key parameters for this modeling include the wire's diameter, sphere size, depletion layer thickness, and the equation governing the wire's shape. The calculations are complex due to the circular cross-section dimensions changing with axial position. Results from these calculations guide the design of ridge and groove dimensions, depletion layer thickness, and undulation wavelengths to enhance particle-groove depositions.

By graphing the excluded volume overlaps for sphere-saddle and sphere-anti-saddle configurations in relation to depletion overlap thickness ($where\ R_s = R_g$), we established design guidelines for enhancing interactions. To promote sphere-saddle depositions instead of sphere-anti-saddle configurations, it is crucial to reduce the size of the smaller particles while maintaining a specific colloid concentration. In summary, the numerical model plays a key role in identifying design parameters and evaluating the size and concentration of smaller particles to optimize shape-selective interactions between particles and grooves.

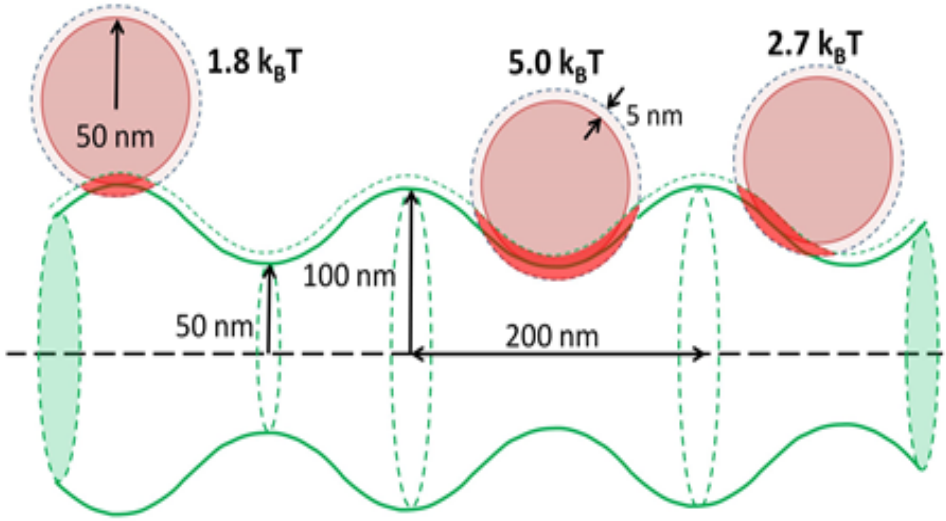

Figure 2.7 The diagram illustrates the interaction between an undulating nanowire (with a radius fluctuating between 50 and 100 nm and a pitch of 200 nm) and a spherical colloid (R_s = 5 nm, R_L = 50 nm, at a small-sphere concentration of 0.38 wt %). The interaction strengths, listed from left to right, are 1.8 k_BT, 5.0 k_BT, and 2.7 k_BT, respectively.

2.3.2 Spherical particles on diameter modulated cylinders

We also conducted modeling studies on nanowires with step changes in diameter, in addition to the previously discussed sinusoidal variations. The choice of diameter-modulated nanowires for these studies is intentional, as researchers have successfully fabricated them using the vapor-liquid-solid (VLS) technique, which relies on adsorption and desorption on the nanowire's sidewalls [85]. Figure 2.9 illustrates how a step change in radius (Δr) leads to an axially symmetric step edge. Our depletion-induced modeling focused on ensuring that particles preferentially deposit at these step edges.

We calculated the interaction strength based on the magnitude of the diameter change (Δr), using the same model parameters (R_L/R_g, R_g and Φ) as in the

sinusoidal nanowire study. The results showed that the interaction strengths were consistently greater than the sphere-cylinder contact strength (refer to Figure 2.6 (d)) for any Δr > 0, due to increased excluded volume overlap between the spherical particles and the step edge structure. The interaction strength exceeded the sphere-cylinder value of 2.39 kBT, except when Δr = 0, where the sphere-cylinder geometry is restored.

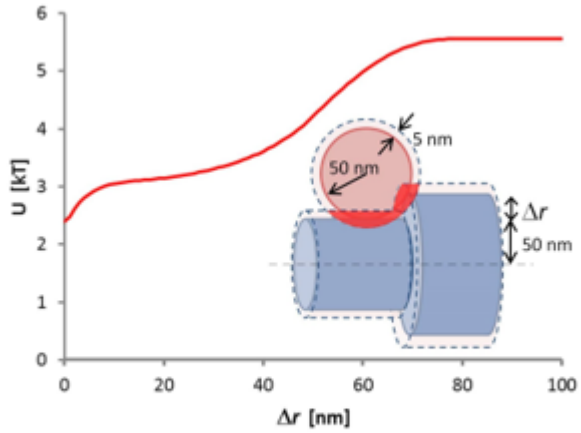

Figure 2.9 The Interaction strength between a spherical colloid (50 nm radius) and a cylindrical nanowire (nominal radius of 50 nm) featuring a step change in radius is analyzed as a function of the radial step size *Δr*, in an aqueous PEG solution (MW = 11,500; R_g = 5 nm) at concentration of 0.38 wt.%.

As anticipated, increasing *Δr* was expected to steadily enhance the excluded volume overlap and interaction potential. However, our plots revealed an unexpected plateau in interaction strength for Δr values between 10 nm and 40 nm. Additionally, as *Δr* increased, the edge structure became more pronounced, further enhancing the excluded overlap volume. At a critical *Δr* of 75 nm, maximum overlap was achieved, and further increases in *Δr* did not yield additional overlap volume.

Although we mathematically explained the observed plateau through detailed numerical analysis, our findings indicate that the intricate geometry of these interactions can result in unexpected calculations of overlap volume and non-intuitive changes in interaction strength as geometrical parameters vary.

2.3.3 Cylinder-cylinder and dumbbell-dumbbell interactions

We expanded our numerical modeling to analyze shape-selective interactions between two non-spherical geometries: cylindrical and dumbbell-shaped particles. Figure 2.10 illustrates the parallel interactions between these structures. While end-to-end interactions yield similar overlap volumes, side-to-side interactions differ significantly due to their shapes. We focused on these side-to-side interactions to explore how to design these particles for selective depletion-induced assembly.

To compute the excluded overlap volumes for various overlap lengths and depletant sizes, we used our numerical model. Due to their smaller overlap volumes from asymmetry, we disregarded dumbbell-cylinder interactions. The calculation of dumbbell-dumbbell overlap volumes is complex because of the additional overlap from the interlocking end-caps (see Figure 2.10). We analyzed the ratio of dumbbell-dumbbell overlap volume (*V(db)*) to cylinder-cylinder overlap volume (*V(cyl)*)as a function of overlap length (x) for a depletant size of 5 nm.

We aimed to identify the ideal overlap length and depletant size to promote interactions between dumbbells rather than cylinders. Our analysis showed that the overlap at the end-cap indent was significant at shorter overlap lengths but decreased with longer lengths. As a result, the ratio of *V(db)/V(cyl)* eached its maximum at shorter overlaps and declined with increasing length. Beyond a critical overlap length of 407 nm, the overlap volume for the cylinder-cylinder configuration surpassed that of the dumbbell-

dumbbell configuration, leading to a *V(db)/V(cyl)* ratio of less than one. This transition occurs because the larger cross-sectional area of the cylinder-cylinder overlap becomes more influential as the overlap length increases.

We also examined the effect of depletant size on these interactions by reproducing plots for two other sizes (2.5 nm and 10 nm) while keeping other dimensions constant. A smaller depletant (2.5 nm) increased the *V(db)/V(cyl)* ratio across all overlap lengths, while a larger size had the opposite effect.

To promote dumbbell-dumbbell interactions, smaller depletant sizes and shorter overlap lengths (below the critical length) are favorable, while higher values favor cylinder-cylinder interactions. Additionally, within mixtures of dumbbells, different orientations can affect specificity. Dumbbells can overlap in parallel or crisscross configurations. To favor one orientation over the other, design rules must be adjusted under fixed conditions or optimum conditions must be identified.

In conclusion, our numerical model successfully identified the optimal conditions for enhancing dumbbell-dumbbell interactions compared to cylinder-cylinder interactions. Future efforts should focus on controlling the preferential orientation of dumbbell geometries.

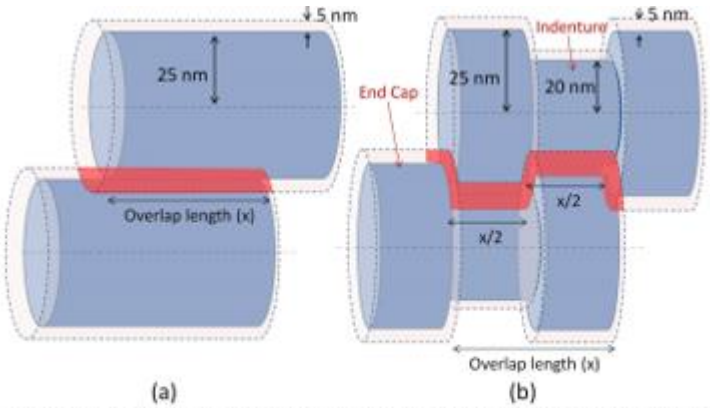

Figure 2.10 A diagram illustrating the side-to-side intersection of (a) cylinder-cylinder and (b) dumbbell-dumbbell geometries. The red shaded areas indicate the regions of excluded volume overlap.

3. Experimental studies

In this section, we present experimental findings of depletion interactions, guided by the modeling studies from the previous section. Our focus is on how polymer concentration (C_p) and electrolyte concentration (C_s) influence the self-assembly of polystyrene (PS) hard-sphere colloids in confined volumes and on structured surfaces. By controlling these two parameters, we can finely adjust the interaction potentials in colloidal systems. The polymer system we use allows us to manipulate both the strength and the range of the attractive potential driving colloid self-assembly. We adjust the depletion interaction strength through C_p (expressed as weight % or volume fraction Φ) and tune the range of electrostatic repulsion through C_s, which controls the ionic strength and screening length (κ^{-1}).

Though previous researchers demonstrated the ability to induce shape-selective interactions, few have examined in detail how electrostatic interactions impact depletion-induced self-assembly [32, 33, 46]. For example, Badaire et al. used lithographically designed cylindrical colloids to control depletion and electrostatic interactions for self-assembly into anisotropic structures 34]. Our aim is to expand upon this by manipulating interactions for various particle and surface geometries.

Hard-sphere colloids, often used as a model system, interact only when in contact, providing a straightforward foundation for studying colloidal

dynamics. However, real hard-sphere systems do not exist. PS colloids are only an approximation, as they are charge-stabilized and deviate from ideal hard spheres. Real materials possess both attractive and repulsive interactions that stabilize them, unlike the idealized hard-sphere systems. Colloids with a combination of these interactions can provide more practical insights into ordered phases [53].

The depletion interaction concept was first noted by Asakura & Osawa (1958), who showed that entropy-driven depletion forces can drive an ordered configuration of large colloidal spheres, resulting in an overall increase in the system's entropy. This is due to the predominance of the entropy of smaller colloids in binary mixtures.

Our investigation focuses on the self-assembly of charged PS colloids and the different types of interactions observed by varying Cp and Cs in the suspension. These interactions are illustrated through a phase diagram detailing the conditions explored. Our emphasis is on understanding and controlling depletion interactions between colloidal particles and surrounding geometries. The strength of depletion interactions is influenced by Cp, while the range of interactions is modulated by the polymer system's radius of gyration (Rg). Larger Rg leads to longer-range interactions but requires a lower polymer number density due to increased excluded volume. Balancing these parameters is crucial to achieving selective depositions on flat and structured surfaces.

Our experimental system consisted of PS spheres and non-adsorbing depleting polymer polyethylene glycol (PEG) in aqueous solutions. PS/PEG colloid-polymer systems have been extensively studied for depletion interactions. PS spheres, being spherical, monodisperse, and commercially available, were ideal for our experiments. The density of PS (1.05 g/cc) allowed for matching with a heavy water-DI water mixture to prevent sedimentation during self-assembly studies. However, their high refractive index (1.59) makes it difficult to observe structures at high densities. To prevent agglomeration, we used surface-modified PS particles with carboxylate groups (-COOH) for charge stabilization. The resulting surface charge (0.3231 C/m²) leads to a Debye double layer, generating electrostatic repulsions that can be screened by adding NaCl to control the ionic strength.

To induce depletion attractions, we used PEG with different molecular weights (MW1 = 1,000,000 Da, Rg ≈ 60 nm; MW2 = 600,000 Da, Rg ≈ 50 nm; MW3 = 20,000 Da, Rg ≈ 7 nm). While MW1 and MW2 resulted in desirable depletion interactions, MW3 was less effective due to the small range of interactions it produced. For charged PS colloids, we used two sizes (0.5 µm and 1 µm). The 1 µm PS colloids showed strong nucleation behavior, while the 0.5 µm particles exhibited weaker interactions, likely due to their higher surface charge (2.5248 C/m² compared to 0.3231 C/m² for the 1 µm particles). The highest screening length achieved was 3 nm, much smaller than the colloid diameters, approximating hard-sphere-like behavior.

The PS particles' behavior was monitored using fluorescence optical microscopy. After preparing polymer and electrolyte stock solutions, mixtures were sonicated for 20 minutes to prevent aggregation, then loaded into 100 µm-thick sample chambers. These chambers were created by placing parafilm spacers between a microscope slide and cover slip, sealed with vacuum grease to prevent evaporation. Approximately 10 µL of suspension was injected into each chamber. Particle behavior was captured in real-time using a Leica DM-IRB microscope with a 63× objective, and images/videos were recorded with a CCD camera at 30 frames/s.

Through these experiments, we explored how depletion and electrostatic interactions can be controlled to direct the self-assembly of colloidal spheres, potentially leading to novel nanostructures and improved understanding of colloidal phase behavior.

3.1 Selective depletion interactions on flat substrates and in bulk

In all our experiments, we employed existing mathematical models to predict how depletion interactions and electrostatic repulsions would affect the charged polystyrene (PS) particles. The values for Cs were chosen such that the Debye screening length was always smaller than the radius of gyration (R_g) of PEG, ensuring that the particles could get close enough for their excluded volumes

to overlap. We used these predictions to guide our choices for polymer and electrolyte concentrations. For the most part, we made sure that the conditions we set up in our experiments were ones where the particles could get close enough together for their shapes to affect each other's movements, which is a requirement for observing any kind of depletion interaction. However, it turns out that predicting just how much energy goes into a depletion interaction is not so simple. We cannot even predict with confidence what the binding energy is between two PS particles when they are in an arrangement where they should be feeling a depletion force. The best we can do is estimate; those estimates are what we've based this discussion on.

Our methodology integrates statistical data from depletion attractions, based on mathematical models, with experimental results to thoroughly comprehend the phenomena. In Section 2, we focused on depletion interactions between colloidal spheres and different wall shapes. Our method started with pinpointing the C_s and C_p that created the most robust interactions and then adjusting these concentrations to get the interactions we wanted. At first, we found the C_s and C_p that caused particles to aggregate and stick together in bulk conditions. After that, we lowered C_s and C_p to find conditions where we got nucleation on a flat surface and then only in bulk conditions.

Our theoretical models predict that crystals will preferentially nucleate at edges rather than on flat surfaces or in the bulk. This behavior is expected because the entropic force acting on a particle near a wall is about twice as large as that between two particles in the bulk, and the entropic force at an edge is about twice as large as that near a wall. However, our initial experiments were conducted on flat glass and silica substrates without sharp edges. There is electrostatic repulsion between the negatively charged carboxylate modified microspheres and the glass or silica substrates, which become negatively charged due to dissociation of silanol groups [83]. For surface nucleation, this repulsion must be overcome by depletion attraction, similar to what occurs during bulk nucleation, where an attractive potential overcomes the repulsive forces between particles.

Figure 3.1(a) shows the usual aggregation of polystyrene (PS) particles due to potent depletion attractions in the bulk. These particle aggregates do not exhibit long range order. When we fine-tuned the concentrations of C_s and C_p, we saw a development in how the PS particles interacted with one another, culminating in disordered aggregates that grew larger and denser as the depletion interactions became stronger. When we further reduced the concentrations of C_s and C_p, we saw something quite different happening in the bulk: dense, 3D crystalline structures formed that had a honeycomb like appearance (Figure 3.1(b)). The strength of interaction between these particles was evidently just right for them to rearrange into an ordered configuration that appears to have minimized the energy of the system. Using a local order parameter, the distinction between aggregates and three dimensional crystals was quantified by measuring their levels of ordering [89].

At intermediate concentrations, we observed sparsely dense clusters lacking orientational ordering due to strong particle-particle interactions. In this regime, particles were bound too strongly to rearrange. As concentrations were further reduced, bulk crystal formation occurred more selectively and spontaneously. At even lower concentrations, bulk activity diminished, and hexagonally symmetric crystalline structures began to form on the wall surface (Figure 3.1 (d)). Here, particle-wall interactions were stronger than particle-particle interactions, preventing crystals from forming in the bulk. These surface crystals, predominantly on the bottom surface due to gravity bias, adhered to the walls and grew over time.

When silica substrates were used as the top confining surface, samples were placed on a slow roller to eliminate the gravity bias that favors interactions on the bottom surface. Large crystals formed at lower depletion potentials showed signs of weak adhesion to the wall, with some diffusing laterally. This indicated that these structures were not deposited in deep kinetic traps, unlike van der Waals interactions, and could be reversibly formed.

At intermediate concentrations between exclusive bulk and surface nucleation, we observed two behaviors. First, a second layer of crystalline structures formed over surface crystals due to strong

particle-particle interactions (Figure 3.1 (c)). Secondly, we saw competition between surface and bulk nucleation, where particles formed either surface or bulk nucleates depending on their initial collisions. This behavior was observed on both glass and silica substrates, with reproducibility confirmed by repeated experiments. The depletion interactions, being material-independent, produced similar results on both substrates.

In some cases, individual PS particles and aggregates bound to the surfaces, likely due to higher C_s values pushing particles closer to surfaces by reducing the repulsive barrier. When Cp was increased beyond the aggregation region, a phase was reached where particles did not interact with themselves or surrounding surfaces. Two theories may explain this phenomenon.

The first theory suggests that the polymer (PEG, MW = 1,000,000 Da) reached its overlap concentration. Water is a good solvent for PEG, with a Flory-Huggins interaction parameter between 0.4–0.5 [79]. The threshold concentration for molecular overlap (C^*)) is related to the polymer's molar mass by $C^* \propto MW^{-4/5}$ [84]. Based on this, we estimated an overlap concentration of 0.138 wt %. At this concentration, depletion attractions appeared to vanish, likely because the polymer formed a mesh structure, shortening the range of interactions and reducing depletion attractions.

The second hypothesis involves entropic repulsion. Dinsmore et al. [45] showed that aggregation kinetics slowed when small particles were more concentrated, with osmotic pressure in narrow gaps causing depletion repulsion. While we lack definitive experimental evidence to confirm either hypothesis, we lean toward the first theory based on the evidence presented. Direct measurements of entropic forces between microspheres would provide a conclusive answer, but such measurements are beyond the scope of this work.

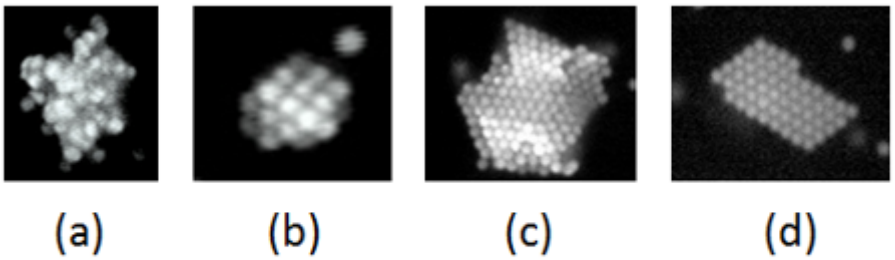

Figure 3.1 Microscopic images of suspensions containing 1 µm diameter particles, displayed in order of decreasing interaction potential. (a) shows aggregation (0.1 wt % PS, 0.082 wt % PEG, 0.05 M NaCl); (b) depicts bulk nucleation (0.1 wt % PS, 0.045 wt % PEG, 0.01 M NaCl); (c) illustrates surface nucleation extending into the bulk (0.1 wt % PS, 0.09 wt % PEG, 0.0325 M NaCl); and (d) presents surface nucleation (0.1 wt % PS, 0.025 wt % PEG, 0.0325 M NaCl).

3.2 Selective depletion interactions on structured surfaces (edges)

The study explores the use of entropic effects in colloid/polymer mixtures to induce particle-particle and particle-wall interactions, extending the concept to structured substrates for particle deposition at specific geometric locations. Prior research has shown that colloidal particles can be trapped at edges, steps, and grooves on substrates if the depletion potential is appropriately tuned [70, 32, 85]. These findings have potential applications in microfabrication via directed self-assembly.

The experiments were conducted on silica substrates due to their relevance in semiconductor fabrication. Grooves were etched onto the silica using the Bosch process, and the dimensions of the structures were measured with scanning profilometry. The aim was to fine-tune the system parameters (C_s, C_p, R_g, R_L) to create selective particle-edge interactions, minimizing particle-particle and particle-wall interactions.

Initial experiments indicated that edge nucleation could be achieved by decreasing Cs and Cp until surface nucleation was absent. Edge crystals were observed before flat surface nucleation. However, achieving highly selective edge nucleation proved challenging due to kinetic limitations and the large surface area of the substrates, which increased the likelihood of particle-wall deposition. To improve

results, neutral buoyancy conditions were created using a mixture of D_2O and H_2O to prevent particle sedimentation.

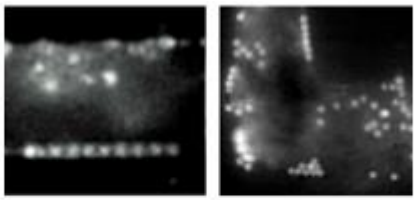

a) b)

Figure 3.3 (a) Displays a linear edge crystal formed along the edge (0.05 wt % PS, 0.015 wt % PEG, 0.015 M NaCl), while (b) shows both linear (top) and edge-surface crystals (0.05 wt % PS, 0.015 wt % PEG, 0.02 M NaCl).

Edge nucleation occurred, but it was rare and slow compared to surface or bulk nucleation, with deposits appearing after 24-48 hours. Crystals forming along the edges did not compare in quality to those on flat surfaces, likely due to surface roughness caused by the Bosch etching process. Surface roughness impacts depletion interactions, as Zhao et al. demonstrated that depletion forces are maximized on smooth surfaces but decrease with increased roughness [87]. The rough sidewalls and undulating surfaces created by the etching process negatively affected the depletion forces.

Another factor limiting edge nucleation was the low concentration of polystyrene (PS) particles used in the experiments. The entropy associated with lower concentrations makes particle-edge deposition more difficult, requiring higher interaction energy to overcome the entropy loss. Increasing the concentration of PS particles could enhance particle-edge collisions, but this was constrained by the limitations of optical microscopy. Dinsmore et al. used a volume fraction of 0.015 to achieve nucleation in corners [32], while this study used 0.005 for edge nucleation and 0.001 for surface nucleation.

There were also instances where crystals that formed along edges diffused onto flat surfaces, making them appear as surface crystals. Some surface crystals observed had a linear boundary, suggesting they may have originally formed along an edge before detaching.

In summary, while the study successfully demonstrated particle-edge nucleation, challenges related to surface roughness, particle concentration, and kinetic limitations affected the process. Further optimization of these parameters could enhance the selectivity and efficiency of edge nucleation for practical applications.

3.5 Phase diagram

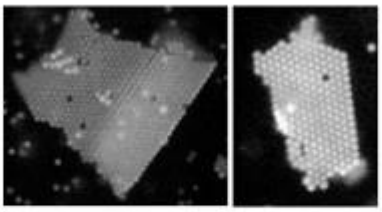

Figure 3.4 Surface crystals observed on structured surfaces featuring linear boundaries on one side (0.1 wt % PS, 0.035 wt % PEG, 0.025 M NaCl).

The phase diagram from systematic experiments shows the depletion interactions by plotting polymer concentration (C_p) on the X axis and salt concentration (C_s) on the Y axis. The regions corresponding to different interactions are color coded, and these colors form patterns that reveal how particles behave under various conditions of C_p and C_s. One of these regions is red; it corresponds to a "stagnation inactivity" condition where C_p or C_s is too low to overcome electrostatic repulsion between particles and surfaces. The first interaction we see in this diagram is edge nucleation, which occurs in a pale blue region. As either C_p or C_s increases, we next observe surface nucleation (green), followed by a yellow region where both surface and bulk nucleation compete. At even higher concentrations, bulk nucleation dominates (blue), and eventually, particle aggregation occurs in the grey region due to van der Waals forces as particles come too close.

The diagram indicates that individual particles and aggregates can still adhere to surfaces during bulk nucleation and aggregation, likely due to weakened electrostatic repulsion. The experimental results align well with numerical modeling, confirming the predicted strength and order of depletion interactions.

Depletion potentials in isotropic spheres exceed 5 kBT [81], but electrostatic repulsion plays a key role in determining the depth of the depletion potential well. Polymer concentration values for which depletion potential reaches 5 kBT were computed for different interactions, and these were marked on the X-axis. Edge nucleation occurred at this threshold, while surface and bulk interactions occurred at lower polymer concentrations as electrolyte concentration increased. This suggests that while particle-wall interactions are weak, particle-particle interactions in a hexagonal lattice stabilize the structure. In bulk nucleation, a honeycomb-like hexagonal close packing (HCP) structure forms, with each particle interacting with twelve others, significantly increasing interaction strength.

In the plot, the phase boundaries look like the hypotenuse of a right triangle. This suggests that electrostatic interactions are as important as depletion interactions in the self-assembly process. The depth of the depletion potential well can increase by two different mechanisms: One is raising the electrolyte concentration, which screens repulsive forces; the other is increasing polymer concentration, which enhances attractive forces. The triangular shape of the phase plot highlights that beyond certain electrolyte or polymer concentrations, specific interactions cease to exist, and others take over. For instance, edge nucleation vanishes above 20 mM electrolyte concentration, likely due to kinetic limitations rather than energetic ones. In this scenario, particles cannot diffuse effectively due to strong surface interactions, preventing further exploration of phase space.

The horizontal transitions in the phase diagram are easier to explain: as polymer concentration increases, interactions become stronger, allowing new interactions to dominate. This is essentially a selectivity effect, where raising electrolyte concentration enables interactions at lower polymer concentrations due to reduced repulsion, making it easier for particles to approach surfaces.

The phase plot reveals that these self assembly systems, driven by entropy, have ideal conditions where the highly selective assembly of particles occurs. This happens at particular concentrations of polymers and electrolytes. Yodh and colleagues previously created a "quasi phase diagram" [58] that delineated regions where surface particles assemble and where bulk complications arise. They indicated these regions using a "liquidus line." However, their model used fixed ionic strength and ignored electrostatic influences, classifying only two types of interactions. In contrast, the phase plot generated here is more comprehensive, capturing a broader range of depletion interactions, making it a valuable tool for investigating these dynamic systems.

3.6 Kinetics of crystallization on flat substrates

To investigate the kinetics of crystallization on flat surfaces, we conducted deposition studies on glass substrates over a period of time. The growth of colloidal crystals, driven by depletion interactions, was observed as a two-step process: the diffusion of particles toward the crystal (a transport step) and their deposition on the crystal (a reaction step). Particles must diffuse and reach the growing crystal to stick, thus contributing to crystal growth. In this

framework, diffusion-limited reactions lead to full aggregation, while reaction-limited reactions lead to weaker interactions.

In some cases, individual particles interacting with the flat substrate may not form stable interactions due to weak binding. However, surface-crystal formation is preferred because particles in the crystal also experience particle-particle interactions, stabilizing the structure. The crystal growth rate was observed on flat surfaces using microscopy. To prevent sedimentation and maintain particle concentration in the bulk, a mixture of D_2O and H_2O was used to create near-neutral buoyancy for the PS colloids. Surface assembly was studied under constant electrolyte concentration but varying PS and PEG volume fractions. These concentrations were chosen based on previous observations as ideal for surface nucleation.

The crystal growth rates were slow, probably because of the low concentration of polystyrene (PS), which reduced the likelihood of particle collisions with the crystal. Growth started with a surface nucleus that appeared spontaneously after introducing a non-adsorbing polymer. This nucleus slowly expanded as particles in the vicinity added to it, forming a hexagonal structure. Although larger nuclei are generally favored thermodynamically and tend to form due to Ostwald ripening, the literature indicates that interaction potentials play a crucial role in determining nucleus size: stronger attractions lead to smaller nuclei, while weaker attractions result in larger ones. Using smaller particles can significantly boost crystallization growth rates because these particles diffuse more readily and rapidly. Their increased diffusivity means they collide with the nucleus more frequently, which in turn raises the overall rate of crystal formation.

In the experiments, higher interaction strength led to the formation of larger crystals, explained by a diffusion-limited reaction mechanism where stronger attractions increase the likelihood of PS-crystal binding. Conversely, weaker interactions follow a reaction-limited mechanism, reducing the likelihood of binding. The crystallization growth rate also increased with higher PS concentrations due to more frequent particle-crystal collisions. However, this increase in particle concentration might also lead to more nucleation sites, though this hypothesis remains unquantified.

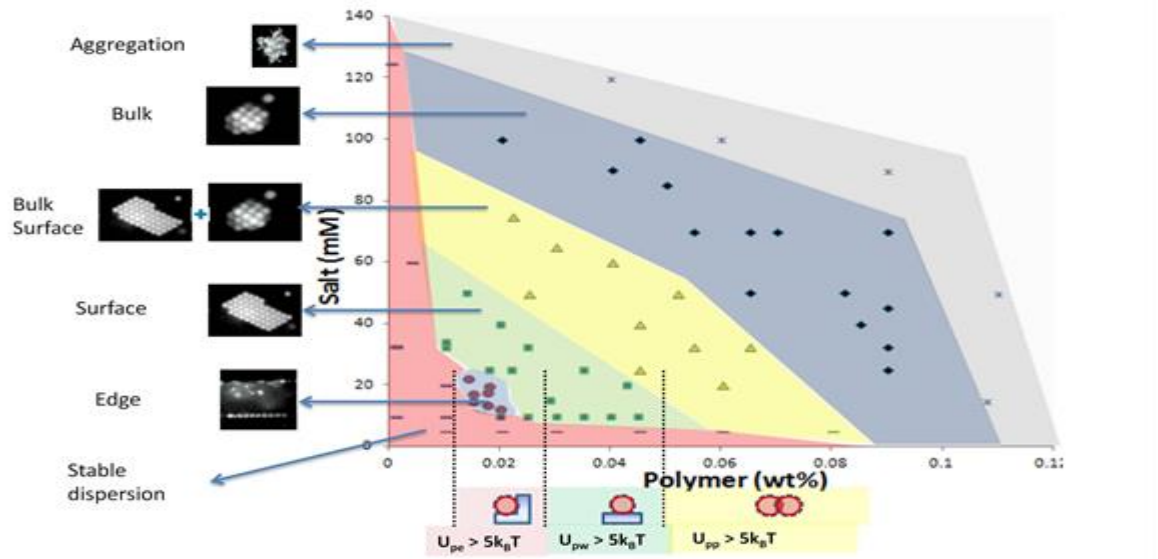

Figure 3.5 A phase plot illustrating all the depletion interactions is presented as a function of electrolyte and polymer concentrations. On the left, each interaction is depicted on the phase plot, while the bottom indicates the positions along the X-axis where each interaction reaches a magnitude of 5 k_BT.

In conclusion, while the results provide insights into crystallization kinetics, further quantitative and qualitative analysis is necessary to better understand the process.

4. Conclusion

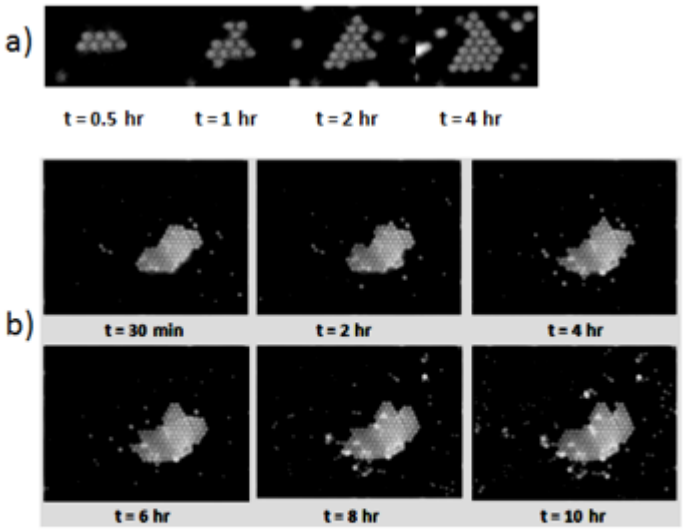

Figure 3.6 A series of fluorescence microscopy images depicting the growth of a depletion-induced colloidal crystal composed of 1 µm diameter fluorescent PS particles in an aqueous PEG solution (MW=1,000,000) on a glass microscope slide are shown for: a) 0.15 wt % PS, 0.02 wt% PEG, 0.05 M NaCl (Upw ~ 4.2 kT) and b) 0.1 wt % PS, 0.025 wt% PEG, 0.05 M NaCl (Upw ~ 6 kT).

This research has explored depletion interactions between colloidal particles and surfaces, combining experimental work with numerical modeling to offer new insights. The depletion interaction potentials for different geometries—such as sphere-sphere, sphere-wall, and sphere-edge—were effectively predicted using a straightforward model. These predictions guided our experimental choices, particularly in adjusting salt (C_s) and polymer (C_p) concentrations. The experimental results closely aligned with the numerical models, validating their use in understanding the interaction strengths. The phase plot generated from these experiments further underscored the role of electrostatic forces, revealing a triangular boundary that links different interactions to polymer and electrolyte concentrations. This triangular relationship, overlooked by previous studies, highlights the balance between electrostatic and depletion forces in these systems.

The experiments confirmed a sequence of interactions, starting with particle-edge nucleation, followed by particle-wall and particle-particle nucleation, and ultimately aggregation. Particle-wall and particle-particle nucleation were readily observed, but particle-edge nucleation was rare, likely due to surface roughness on the silica substrates, which inhibited the interaction. This suggests that surface smoothness plays a critical role in controlling the precision of selective particle deposition.

The rate of surface crystal growth was also examined, revealing that the strength of depletion forces and the volume fraction of particles influence the growth process. Although more detailed analysis is required, the results suggest that these factors could be optimized to better control self-assembly on surfaces.

While the focus of this study was on reversible particle deposition, it is crucial to explore methods for permanently binding particles to surfaces for practical applications. Future studies should consider methods like mild annealing above the polymer glass transition temperature to solidify the assembled structures. For example, heating polystyrene (PS) particles in ethylene glycol has

been shown to fuse the particles into stable coatings, which could offer a path forward for creating durable, self-assembled materials. This research lays the groundwork for further studies aimed at improving the control and permanence of depletion-driven particle assemblies in various applications.

References

1. Hotze, E.M., T. Phenrat, and G.V. Lowry, *Nanoparticle aggregation: Challenges to understanding transport and reactivity in the environment.* Journal of environmental quality, 2010. **39**: p. 1909-1924.
2. Ivanov, I.B., K.D. Danov, and P.A. Kralchevsky, *Flocculation and coalescence of micron-size emulsion droplets.* Colloids and Surfaces A: Physicochemical and Engineering Aspects, 1999. **152**(1–2): p. 161-182.
3. Dimiter, P., *Emulsions: Structure, stability and interactions*. 2004: Academic Press.
4. Derjaguin, B. and L. Landau, *Theory of the stability of strongly charged lyophobic sols and of the adhesion of strongly charged particles in solutions of electrolytes.* Progress in Surface Science, 1993. **43**(1–4): p. 30-59.
5. Verwey, E.J.W., *Theory of the stability of lyophobic colloids.* The Journal of Physical and Colloid Chemistry, 1947. **51**(3): p. 631-636.
6. Israelachvili, J.N., *6 - Van der Waals Forces*, in *Intermolecular and surface forces (third edition)*, J.N. Israelachvili, Editor. 2011, Academic Press: San Diego. p. 107-132.
7. Van Der Hoeven, P.C. and J. Lyklema, *Electrostatic stabilization in non-aqueous media.* Advances in Colloid and Interface Science, 1992. **42**(0): p. 205-277.
8. Roberts, G.S., et al., *Electrostatic charging of nonpolar colloids by reverse micelles.* Langmuir, 2008. **24**(13): p. 6530-6541.
9. Gregory, J., *Interaction of unequal double layers at constant charge.* Journal of Colloid and Interface Science, 1975. **51**(1): p. 44-51.
10. Asakura, S. and F. Oosawa, *Interaction between particles suspended in solutions of macromolecules.* Journal of Polymer Science, 1958. **33**(126): p. 183-192.
11. Lekkerkerker, H.N.W. and R. Tuinier, *Colloids and the depletion interaction*. 2011: Springer.
12. Israelachvili, J.N. and R.M. Pashley, *Molecular layering of water at surfaces and origin of repulsive hydration forces.* Nature, 1983. **306**(5940): p. 249-250.
13. Israelachvili, J. and H. Wennerstrom, *Role of hydration and water structure in biological and colloidal interactions.* Nature, 1996. **379**(6562): p. 219-225.
14. Clunie, J.S., J.F. Goodman, and P.C. Symons, *Solvation forces in soap films.* Nature, 1967. **216**(5121): p. 1203-1204.
15. Mueller, S., E.W. Llewellin, and H.M. Mader, *The rheology of suspensions of solid particles*. Vol. 466. 2010. 1201-1228.
16. Royall, C.P., W.C.K. Poon, and E.R. Weeks, *In search of colloidal hard spheres.* Soft Matter, 2013. **9**(1): p. 17-27.
17. Vlassopoulos, D. and M. Cloitre, *Bridging the gap between hard and soft colloids.* Soft Matter, 2012. **8**(15): p. 4010-4013.
18. Jose, J., G.A. Blab, A. van Blaaderen, and A. Imhof, *Jammed elastic shells - a 3D experimental soft frictionless granular system.* Soft Matter, 2015. **11**(9): p. 1800-1813.
19. Brenner, H., *The slow motion of a sphere through a viscous fluid towards a plane surface.* Chemical Engineering Science, 1961. **16**(3–4): p. 242-251.
20. Edwards, S.A., S.L. Carnie, O. Manor, and D.Y.C. Chan, *Effects of internal flow and viscosity ratio on measurements of dynamic forces between deformable drops.* Langmuir, 2009. **25**(6): p. 3352-3355.
21. Cheremisinoff, N.P., *1 - An introduction to liquid filtration*, in *Liquid Filtration (Second Edition)*, N.P. Cheremisinoff, Editor. 1998, Butterworth-Heinemann: Woburn. p. 1-18.
22. McDowell-Boyer, L.M., J.R. Hunt, and N. Sitar, *Particle transport through porous media.* Water Resources Research, 1986. **22**(13): p. 1901-1921.
23. Pamme, N., *Continuous flow separations in microfluidic devices.* Lab on a Chip, 2007. **7**(12): p. 1644-1659.

24. Goldman, A.J., R.G. Cox, and H. Brenner, *The slow motion of two identical arbitrarily oriented spheres through a viscous fluid.* Chemical Engineering Science, 1966. **21**(12): p. 1151-1170.
25. MacKintosh, F.C. and C.F. Schmidt, *Microrheology.* Current Opinion in Colloid & Interface Science, 1999. **4**(4): p. 300-307.
26. Waigh, T.A., *Microrheology of complex fluids.* Reports on Progress in Physics, 2005. **68**(3): p. 685.
27. Mason, T.G. and D.A. Weitz, *Optical measurements of frequency-dependent linear viscoelastic moduli of complex fluids.* Physical Review Letters, 1995. **74**(7): p. 1250-1253.
28. Chung, K., et al., *Three-dimensional in situ temperature measurement in microsystems using Brownian motion of nanoparticles.* Analytical Chemistry, 2009. **81**(3): p. 991-999.
29. Crocker, J.C. and D.G. Grier, *Methods of digital video microscopy for colloidal studies.* Journal of Colloid and Interface Science, 1996. **179**(1): p. 298-310.
30. Cheezum, M.K., W.F. Walker, and W.H. Guilford, *Quantitative comparison of algorithms for tracking single fluorescent particles.* Biophysical Journal, 2001. **81**(4): p. 2378-2388.
31. Breedveld, V. and D.J. Pine, *Microrheology as a tool for high-throughput screening.* Journal of Materials Science, 2003. **38**(22): p. 4461-4470.
32. Dinsmore, A.D. and A.G. Yodh, *Entropic confinement of colloidal spheres in corners on silicon substrates.* Langmuir, 1999. **15**(2): p. 314-316.
33. Lin, K.H., et al., *Entropically driven colloidal crystallization on patterned surfaces.* Physical Review Letters, 2000. **85**(8): p. 1770-1773.
34. Badaire, S., et al., *Shape selectivity in the assembly of lithographically designed colloidal particles.* Journal of the American Chemical Society, 2007. **129**(1): p. 40-41.
35. Churaev, N.V. and V.D. Sobolev, *Surface forces in nanostructures*, in *Nanoscience*. 2010, CRC Press. p. 3-29.
36. N'guessan, H.E., et al., *Water tribology on graphene.* Nat Commun, 2012. **3**: p. 1242.
37. Akbulut, M., *Nanoparticle-based lubrication systems.* Journal of Powder Metallurgy & Mining, 2012.
38. Roca, J.F. and M.S. Carvalho, *Flow of a drop through a constricted microcapillary.* Computers & Fluids, 2013. **87**(0): p. 50-56.
39. Fidalgo, L.M., et al., *From microdroplets to microfluidics: Selective emulsion separation in microfluidic devices.* Angewandte Chemie International Edition, 2008. **47**(11): p. 2042-2045.
40. Shah, R.K., et al., *Fabrication of monodisperse thermosensitive microgels and gel capsules in microfluidic devices.* Soft Matter, 2008. **4**(12): p. 2303-2309.
41. Magnaudet, J., S. takagi, and D. legendre, *Drag, deformation and lateral migration of a buoyant drop moving near a wall.* Journal of Fluid Mechanics, 2003. **476**: p. 115-157.
42. Collier, J.H., et al., *Thermally and photochemically triggered self-assembly of peptide hydrogels.* Journal of the American Chemical Society, 2001. **123**(38): p. 9463-9464.
43. Strong, M., *Protein nanomachines.* PLoS Biol, 2004. **2**(3): p. e73.
44. Minton, A.P., *Confinement as a determinant of macromolecular structure and reactivity. II. Effects of weakly attractive interactions between confined macrosolutes and confining structures.* Biophysical Journal, 1995. **68**(4): p. 1311-1322.
45. Crocker, J.C., J.A. Matteo, A.D. Dinsmore, and A.G. Yodh, *Entropic attraction and repulsion in binary colloids probed with a line optical tweezer.* Physical Review Letters, 1999. **82**(21): p. 4352-4355.
46. Sacanna, S., W.T.M. Irvine, P.M. Chaikin, and D.J. Pine, *Lock and key colloids.* Nature, 2010. **464**(7288): p. 575-578.
47. Marenduzzo, D., K. Finan, and P.R. Cook, *The depletion attraction: an underappreciated force driving cellular organization.* The Journal of Cell Biology, 2006. **175**(5): p. 681-686.
48. Gast, A.P. and W.B. Russel, *Simple ordering in complex fluids - Colloidal particles suspended in solution provide*

intriguing models for studying phase transitions. Physics Today, 1998. **51**(12): p. 24-30.
49. Iracki, T.D., D.J. Beltran-Villegas, S.L. Eichmann, and M.A. Bevan, *Charged micelle depletion attraction and interfacial colloidal phase behavior*. Langmuir, 2010. **26**(24): p. 18710-18717.
50. Vrij, A., *Polymers at interfaces and the interactions in colloidal dispersions.* Pure and Applied Chemistry, 1976. **48**(4): p. 471-483.
51. Ricci, F., A. Vallee-Belisle, and K.W. Plaxco, *High-precision, in vitro validation of the sequestration mechanism for generating ultrasensitive dose-response curves in regulatory networks.* Plos Computational Biology, 2011. **7**(10): p. 8.
52. Dickman, R., P. Attard, and V. Simonian, *Entropic forces in binary hard sphere mixtures: Theory and simulation.* Journal of Chemical Physics, 1997. **107**(1): p. 205-213.
53. Yodh, A.G., et al., *Entropically driven self–assembly and interaction in suspension*. Vol. 359. 2001. 921-937.
54. Singh, R.P., et al., *Biobased polymeric flocculants for industrial effluent treatment.* Materials Research Innovations, 2003. **7**(5): p. 331-340.
55. Sierra-Martin, B., et al., *Microscopic signature of a microgel volume phase transition.* Macromolecules, 2005. **38**(26): p. 10782-10787.
56. Rosenberger, F., *Protein crystallization.* Journal of Crystal Growth, 1996. **166**(1-4): p. 40-54.
57. Dickinson, E., *Special issue: Food emulsions and foams: Interfaces, interactions and stability*. Colloids and Surfaces B-Biointerfaces, 1999. **12**(3-6): p. 105-105.
58. Talapin, D.V., J.S. Lee, M.V. Kovalenko, and E.V. Shevchenko, *Prospects of colloidal nanocrystals for electronic and optoelectronic applications.* Chemical Reviews, 2010. **110**(1): p. 389-458.
59. Gast, A.P., C.K. Hall, and W.B. Russel, *Polymer-induced phase separations in non-aqueous colloidal suspensions.* Journal of Colloid and Interface Science, 1983. **96**(1): p. 251-267.
60. Piasecki, J., L. Bocquet, and J.P. Hansen, *Multiple time-scale derivation of the Fokker-Planck equation for 2 Brownian spheres suspended in a hard-sphere fluid.* Physica A, 1995. **218**(1-2): p. 125-144.
61. Biben, T., P. Bladon, and D. Frenkel, *Depletion effects in binary hard-sphere fluids.* Journal of Physics-Condensed Matter, 1996. **8**(50): p. 10799-10821.
62. Chu, X.L., A.D. Nikolov, and D.T. Wasan, *Effects of particle size and polydispersity on the depletion and structural forces in colloidal dispersions.* Langmuir, 1996. **12**(21): p. 5004-5010.
63. Gotzelmann, B., R. Evans, and S. Dietrich, *Depletion forces in fluids.* Physical Review E, 1998. **57**(6): p. 6785-6800.
64. Bechinger, C., et al., *Understanding depletion forces beyond entropy.* Physical Review Letters, 1999. **83**(19): p. 3960-3963.
65. Rudhardt, D., C. Bechinger, and P. Leiderer, *Repulsive depletion interactions in colloid-polymer mixtures.* Journal of Physics-Condensed Matter, 1999. **11**(50): p. 10073-10078.
66. Sharma, A. and J.Y. Walz, *Direct measurement of the depletion interaction in a charged colloidal dispersion.* Journal of the Chemical Society-Faraday Transactions, 1996. **92**(24): p. 4997-5004.
67. Sober, D.L. and J.Y. Walz, *Measurement of long range depletion energies between a colloidal particle and a flat surface in micellar solutions.* Langmuir, 1995. **11**(7): p. 2352-2356.
68. Van Helden, A.K., J.W. Jansen, and A. Vrij, *Preparation and characterization of spherical monodisperse silica dispersions in nonaqueous solvents.* Journal of Colloid and Interface Science, 1981. **81**(2): p. 354-368.
69. Sharma, A. and J.Y. Walz, *Direct measurement of the depletion interaction in a charged colloidal dispersion.* Journal of the Chemical Society, Faraday Transactions, 1996. **92**(24): p. 4997-5004.
70. Dinsmore, A.D., A.G. Yodh, and D.J. Pine, *Entropic control of particle motion using*

passive surface microstructures. Nature, 1996. **383**(6597): p. 239-242.
71. Wall, F.T., *Principles of polymer chemistry. Paul J. F.. Cornell Univ. Press, Ithaca, New York, 1953. 688 pp. Illus. $8.50.* Science, 1954. **119**(3095): p. 555-556.
72. Bower, D.I., *An introduction to polymer physics*. 2002: Cambridge University Press.
73. Meijer, E.J. and D. Frenkel, *Colloids dispersed in polymer-solutions - a computer-simulation study.* Journal of Chemical Physics, 1994. **100**(9): p. 6873-6887.
74. Joanny, J.F., L. Leibler, and P.G. Degennes, *Effects of polymer-solutions on colloid stability.* Journal of Polymer Science Part B-Polymer Physics, 1979. **17**(6): p. 1073-1084.
75. Eric, W. *Circle-circle intersection*. 1999; Available from: http://mathworld.wolfram.com/Circle-CircleIntersection.html.
76. Rudhardt, D., C. Bechinger, and P. Leiderer, *Direct measurement of depletion potentials in mixtures of colloids and nonionic polymers.* Physical Review Letters, 1998. **81**(6): p. 1330-1333.
77. Weronski, P., J.Y. Walz, and M. Elimelech, *Effect of depletion interactions on transport of colloidal particles in porous media.* Journal of Colloid and Interface Science, 2003. **262**(2): p. 372-383.
78. Devanand, K. and J.C. Selser, *Asymptotic behavior and long-range interactions in aqueous solutions of poly(ethylene oxide).* Macromolecules, 1991. **24**(22): p. 5943-5947.
79. Lee, J.H., H.B. Lee, and J.D. Andrade, *Blood compatibility of polyethylene oxide surfaces.* Progress in Polymer Science, 1995. **20**(6): p. 1043-1079.
80. Musin, I.R., N. Shin, and M.A. Filler, *Diameter modulation as a route to probe the vapour-liquid-solid growth kinetics of semiconductor nanowires.* Journal of Materials Chemistry C, 2014. **2**(17): p. 3285-3291.
81. Alder, B.J. and T.E. Wainwright, *Phase transition for a hard sphere system.* The Journal of Chemical Physics, 1957. **27**(5): p. 1208-1209.
82. Prasad, V., D. Semwogerere, and E.R. Weeks, *Confocal microscopy of colloids.* Journal of Physics-Condensed Matter, 2007. **19**(11): p. 25.
83. Behrens, S.H. and D.G. Grier, *The charge of glass and silica surfaces.* The Journal of Chemical Physics, 2001. **115**(14): p. 6716-6721.
84. Borba, J.R., et al., *Quantitative characterization of hexagonal packings in nanoporous alumina arrays: A case study.* Journal of Physical Chemistry C, 2013. **117**(1): p. 246-251.
85. Dinsmore, A.D., D.T. Wong, P. Nelson, and A.G. Yodh, *Hard spheres in vesicles: Curvature-induced forces and particle-induced curvature.* Physical Review Letters, 1998. **80**(2): p. 409-412.